buildings

MDPI

Article

Experimental and Numerical Characterization of the In-Plane Shear Behavior of a Load-Bearing Hollow Clay Brick Masonry System with High Thermal Performance

Michele Serpilli [1,*], Alessandro Cameli [1] and Francesca Stazi [2]

[1] Department of Civil and Building Engineering, and Architecture (DICEA), Università Politecnica delle Marche, 60131 Ancona, Italy; a.cameli@univpm.it
[2] Department of Materials, Environmental Sciences and Urban Planning (SIMAU), Università Politecnica delle Marche, 60131 Ancona, Italy; f.stazi@univpm.it
* Correspondence: m.serpilli@univpm.it

Abstract: Modern masonry systems are generally built with hollow clay bricks with high thermal insulating properties, fulfilling the latest sustainability and environmental criteria for constructions. Despite the growing use of sustainable masonries in seismic-prone countries, there is a notable lack of experimental and numerical data on their structural behavior under lateral in-plane loads. The present study investigates the in-plane shear behavior of load-bearing masonry walls with thin bed joints and thermal insulating hollow clay blocks. Shear-compression tests were performed on three specimens to obtain information about their shear strength, displacement capacity and failure modes. The experimental characterization was supplemented by three shear tests on triplets, along with flexural and compression tests on the mortar for the thin joints. Furthermore, two Finite Element (FE) models were built to simulate the shear-compression tests, considering different constitutive laws and brick-to-brick contact types. The numerical simulations were able to describe both the shear failure modes and the shear strength values. The results showed that the experimental shear strength was 53% higher than the one obtained through Eurocode 6. The maximum shear load was found to be up to 75% greater compared to similar masonry specimens from the literature. These findings contribute to a better understanding of the potential structural applications of sustainable hollow clay block masonry in earthquake-prone areas.

Keywords: thermal insulating masonry; shear-compression tests; Finite Element analysis; seismic behavior

Citation: Serpilli, M.; Cameli, A.; Stazi, F. Experimental and Numerical Characterization of the In-Plane Shear Behavior of a Load-Bearing Hollow Clay Brick Masonry System with High Thermal Performance. *Buildings* **2024**, *14*, 2903. https://doi.org/10.3390/buildings14092903

Academic Editors: Duc-Kien Thai, Yiyi Zhou and Zhengyi Kong

Received: 30 July 2024
Revised: 9 September 2024
Accepted: 12 September 2024
Published: 14 September 2024

1. Introduction

The past two decades have seen increasingly rapid advances in the field of innovative and sustainable constructions in order to mitigate their significant impact on global energy consumption [1]. The other key factor affecting the sustainability of buildings is their remarkable carbon emissions throughout their lifetime [2]. According to this perspective, the masonry market, for one of the oldest construction systems, has witnessed rapid technologic development in recent years. The main innovations concern the use of innovative and yet sustainable blocks and joints, aiming to increase their thermal efficiency and lower their construction environmental impact. With the aim of spreading the use of more sustainable and eco-friendly construction materials, recent studies have explored the employment of different types of block units, such as earthen [3,4], residual soil [5] and calcium silicate bricks [6,7]. Furthermore, the thermal and structural performance have been found to improve when incorporating several natural and industrial waste products (e.g., concrete waste, steel fibers, wooden fibers, etc.) into unfired clay bricks [8,9]. Concerning masonry bed joints, a variety of studies have focused on modern bonding systems, aiming to reduce the extent of thermal bridges and the brick-laying time. Different materials have been

investigated for these joints, such as polyurethan foam [10–12], polymer products [13], fiber-reinforced mortar [14] and polymer–cement [15].

Due to the aforementioned advancements in masonry constructions, complying in terms of both their thermal and environmental performance, new types of masonry structural systems have emerged and been employed in countries prone to seismic hazards. Among the wide variety of masonries, those made of load-bearing hollow or multi-perforated bricks are the most widespread in earthquake-prone areas, in Europe [16,17] and in other countries [18,19]. Thus, an in-depth analysis of their seismic performance and an understanding of their shear behavior are crucial for industrial construction purposes and to provide guidelines for future technical regulations [20]. To evaluate the in-plane shear behavior of walls under more realistic seismic conditions and simultaneously obtain indications of their displacement capacity and failure modes, shear-compression tests represent the most valid option. These tests are carried out by subjecting the specimens to a constant vertical force and horizontal monotonic or cyclic lateral forces until failure. Vertical precompression is able to reproduce the static load state experienced by the wall, while the varying lateral force simulates the excitation generated by seismic forces and activates the in-plane damage mechanisms. Several papers have been devoted to investigating the in-plane shear capacity of load-bearing masonry walls made with hollow or perforated block units in unreinforced [7,16,21–25], reinforced [26,27] and confined configurations [28,29], respectively. The majority of the above studies assessed not only the structural performance of the walls but also that of their elements (bricks, mortar and joints). In general, the experimental results in terms of shear strength and ultimate drift were strongly influenced by the mechanical properties of the constituent materials (bricks and mortar), constraint conditions, vertical precompression load and dimensions of the specimens (slenderness and/or aspect ratios). Moreover, the main failure modes (flexural, diagonal and sliding shear) strictly depend on the wall's size and scale and especially on the type of mortar bed joint. For a detailed review on the in-plane shear behavior of masonry walls, their resistant mechanisms and the existing design formulations for their in-plane strength, readers can refer to [30] and the references therein.

Regarding numerical studies, significant advances have been made in numerical modeling of the in-plane shear behavior of masonry. The Finite Element (FE) method is a very useful tool for evaluating the response of masonry structures, as it allows for the study of their behavior at different scales. The key modeling approaches employing FEs are the macro-modeling approach [31–36], the simplified micro-modeling approach [37–39] and the detailed micro-modeling approach [40,41]. Although they are very powerful and efficient, refined computational models are too complex for everyday engineering practice, and the use of simple but effective FE tools can be considered more advantageous, especially when studying small-scale structures.

Even though wall testing provides valuable insights, further experimental and numerical programs are needed to characterize the in-plane shear behavior of innovative masonry panels with specific hollow and perforated block units at different scales and with distinct mortar joints.

The present study aims to contribute to the growing knowledge about hollow load-bearing masonries with thermal insulating properties by providing a detailed structural characterization of small-size specimens. The technology investigated consists of hollow load-bearing bricks with recycled wood powder added and bonded to each other with horizontal thin layers of a special mortar (see Sections 2 and 3 for more details). The structural characterization was carried out in three phases: experimental; numerical; and analytical. Shear-compression tests were performed on three scaled masonry walls under a lateral monotonically increasing load and a constant vertical load, simulating the base wall of a three-story building. In addition, compression and flexural tests were carried out on mortar samples to experimentally establish the shear strength of the special compound according to EN 1015-11:2019 [42]. Finally, three shear tests on triplets were performed, following EN 1052-3:2002/A1:2007 [43], aiming to assess the stress–strain relationship of

the horizontal joints. The shear-compression tests were performed on scaled masonry specimens built with full-size bricks. Despite the scaling effect possibly affecting the strength and stiffness values, these deviations can be considered acceptable [44–46]. Nonlinear static FE analyses, aiming to obtain detailed insight into the stress–strain relationships within the masonry and predict the behavior of the masonry under different loading conditions, were performed. Moreover, the strength and drift parameters of the walls under the test conditions were calculated analytically based on Eurocode 6 [47] and Eurocode 8 [48]. Finally, a comparison between the present research and other experimental campaigns on the in-plane shear-compression behavior of hollow clay brick masonry walls is reported.

2. Research Significance

This section gives more detailed insights into the novelty of the present study on a particular masonry system. In the context of innovative masonry constructions recently used in seismic-prone areas, Porotherm technology offers various solutions for addressing the problem of low environmental sustainability in buildings [49]. Porotherm bricks are clay blocks with vertical and/or horizontal hollows intended for structural and non-structural walls with high insulating properties. Several waste products can be added to the clay in order to minimize their environmental impact and increase their performance, such as coal ash, rice husk, granite slurry or wood powder (see Section 3). The bonding of the bricks, which represents a key element for the stress distribution in the wall, is ensured by an interlocking system and mortar infills (for vertical joints) and thin bed joints. Most research programs have focused on the thermal and environmental performance of this masonry technology (see, e.g., [50–52]). A few scientific works have addressed structural characterization of their in-plane shear strength, displacement capacity and failure modes. For instance, in Lu and Kasa [53], their cyclic shear-compression and diagonal tests on scaled walls, supported by shacking table tests on a real-scale specimen, led to an assessment of the safety of the system in seismic-prone areas. In particular, no significant damage was observed when reproducing seismic conditions corresponding to acceleration of up to 0.74 g. Morandi et al. [54] underlined the necessity of further investigations on the mechanical characterization of load-bearing masonries built with hollow clay insulating bricks and thin bed joints. Mendes et al. [55] carried out a shaking table test on a real-scale mock-up building built with a Porotherm system (200 mm thick bricks), observing a combination of shear, sliding and local crush failures. The drift values were found to be comparable or higher to those reported in Eurocode 8 [48]. Partene et al. [56] evaluated the shear capacity of Porotherm brick walls under seismic excitation in unreinforced and reinforced configurations, highlighting the corresponding diagonal cracking and sliding of the horizontal bed joints. Shermer et al. [57] performed an extensive experimental shear test campaign on full-story-height masonry wall specimens of high-precision thermally insulated clay masonry units, highlighting their structural performance and consistency with the current codes. More recently, Qin et al. [29] studied the cyclic seismic behavior of unreinforced and confined masonry walls using innovative sintered insulation shale blocks: the results pointed out the better performance in terms of their failure mechanism, hysteretic performance, deformation and strength capacity of the confined walls with respect to the unreinforced ones.

Although some structural characterizations have been conducted on these new masonry systems, the existing research on Porotherm load-bearing masonry systems with thin bed joints is relatively limited and requires further investigations. In particular, mechanical characterization of the technology studied, based on the seismic response of this innovative structural system, can lead to new useful insights into the design of sustainable masonry structures.

3. Materials

The masonry system under investigation is made of Porotherm BIO PLAN 45-25/19.9 load-bearing blocks and Porotherm special mortar, both produced by Wienerberger S.p.a, Italy.

3.1. Block Units

The blocks (see Figure 1), manufactured with the addition of wood powder, are rectified on their top and bottom faces and have a male–female interlocking system on their vertical faces, with dimensions of 450 mm (thickness) × 250 mm (length) × 199 mm (height). The particular shape of their vertical faces facilitates the brick-laying process. The percentage of void areas, resulting from the vertically oriented holes, is lower than 45%. The percentage of void areas in the blocks is a key factor in masonries, impacting both their structural [58] and thermal performance [50]. The thickness of the webs and shells is compliant with EN 771-1:2011+A1:2015 [59]. Furthermore, the block units present high thermal efficiency characteristics. Indeed, the presence of wood powder allows the bricks to reach a thermal conductivity of 0.12 W/mK, in accordance with EN 1745:2020 [60]. The low thermal conductivity of the bricks and the reduced thermal bridges facilitated by their thin joints reflects their benefits for the equivalent thermal conductivity of the wall, equal to 0.12 W/mK. Consequently, with this technology, the walls acquire a thermal transmittance of 0.255 W/m^{2}K, neglecting the plaster. The periodic thermal transmittance and the internal areal heat capacity are 0.003 W/m^{2}K and 40.30 kJ/m^{2}K (considering internal and external lime plaster of a 20 mm thickness). The mechanical properties of the Porotherm BIO PLAN 45 bricks are listed in Table 1.

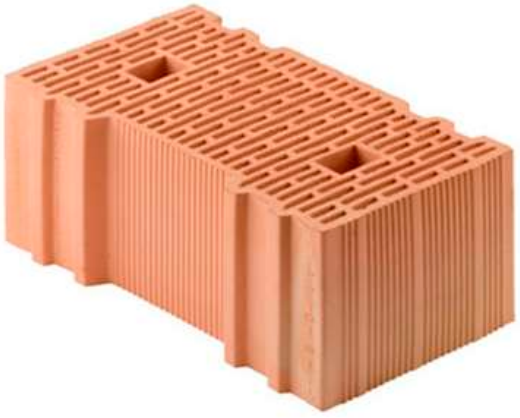

Figure 1. Porotherm BIO PLAN 45-25/19.9.

Table 1. Mechanical properties of Porotherm BIO PLAN 45.

Mean density	(kg/m^3)	970
Vertical compression characteristic strength (f_{bk})	(N/mm^2)	12
Horizontal compression characteristic strength (f_{hk})	(N/mm^2)	3

3.2. Special Mortar

The high-fluidity Porotherm special mortar allows the use of thin horizontal joints (1 mm thick). The pre-mixed mortar powder was added to water, following the specifications of the producer company, and stirred until a high level of workability was reached. The special mortar is classified as M10 [61]. Vertical pockets resulting from the assembly of the masonry were filled with regular M10 structural mortar. Figure 2 shows the mixing of the Porotherm special mortar. The mechanical properties of the Porotherm special mortar are reported in Table 2.

Figure 2. Preparation of Porotherm special mortar.

Table 2. Mechanical properties of Porotherm special mortar from technical data sheet.

Dry density	(kg/m^3)	1200
Compression strength	(N/mm^2)	>10

3.3. Wall Specimen Construction

The walls were built according to the indications of the producing company (Figure 3). The first row of bricks was laid by placing them side by side, filling the empty intermediate vertical pockets with regular mortar. The special mortar was applied by dipping the bottom faces of the bricks into it before laying them, ensuring a bed joint thickness of 1 mm. The structural properties of the masonry system are listed in Table 3, according to the technical specifications provided by the producer.

(**a**) (**b**) (**c**)

Figure 3. Application of special mortar to horizontal thin joints (**a**); application of regular structural mortar to the head joints (**b**); brick-laying process of a wall (**c**).

Table 3. Structural properties of masonry built with Porotherm BIO PLAN 45 and Porotherm special mortar from technical data sheet.

Mean density	(kg/m^3)	974
Compression characteristic strength (f_k) *	(N/mm^2)	7.2
Shear characteristic strength (f_{vok}) *	(N/mm^2)	3

* Mechanical strength values derived by extension from laboratory certificates.

4. Methods

4.1. The Experimental Program

The experimental program consisted of three structural characterization tests:

- Lateral shear-compression tests on three masonry walls;
- Bending and compression tests on three Porotherm mortar specimens;
- Triplet shear tests on three masonry specimens.

4.1.1. Shear-Compression Tests

Three walls (W01, W02, W03) with dimensions of 1250 mm (width) × 1190 mm (height) × 450 mm (thickness) were built at the Laboratorio Ufficiale Prove Materiali e Strutture "Prof. G. Menditto" (LPMS) of the Università Politecnica delle Marche. The specimens were subjected to in-plane lateral load tests under vertical precompression. The aim of the tests was to obtain insights into the structural behavior of the walls under seismic conditions. In particular, it was possible to obtain the shear strength and the deformation capacity of the specimens from their respective τ (shear stress)–γ (shear strain) curves.

The walls, located under the laboratory frame, were supported on the ground and constrained against horizontal displacement at the base. Vertical precompression was applied using two hydraulic jacks (max. load of 500 kN each) placed on the top of the masonry panels and fixed to the laboratory steel frame. The vertical load was applied to a steel plate (500 mm × 1200 mm × 25 mm) and placed on top of seven smooth steel cylinders (∅30) sliding in an L-shaped steel profile (500 mm × 1200 mm × 25 mm), guaranteeing the uniform distribution of the precompression load on the wall's upper side and the free shear deformation of the masonry panel. The hydraulic jacks were connected to a hydraulic control unit with a pressure transducer, enabling measurement of the applied force. The precompression value of 0.62 N/mm^2 was kept constant throughout the lateral load test to simulate the vertical compression endured by a load-bearing wall at the base of a three-story building. The lateral load was applied to the plane of the wall, at the top on the vertical side of the L-shaped steel profile, and increased monotonically until failure. The lateral load was applied by means of a hydraulic jack (max. load 500 kN) connected to a control unit.

Five linear variable displacement transducers (LVDTs) were applied to the masonry panels. The horizontal displacement of the wall was recorded by the horizontal LVDT (O1) placed at the top of the wall. Possible rocking and flexural mechanisms of the wall were assessed through the vertical displacements of the left bottom corner, right under the horizontal hydraulic jack, measured by the vertical LVDT (V1). Possible slippage at the base of the wall was measured by the horizontal LVDT placed at the right bottom corner (O2). The shear strain along the diagonal struts under tension and compression was measured by two diagonal LVDTs (D1, D2); see Figure 4. The complete setup of the shear-compression tests is shown in Figure 5.

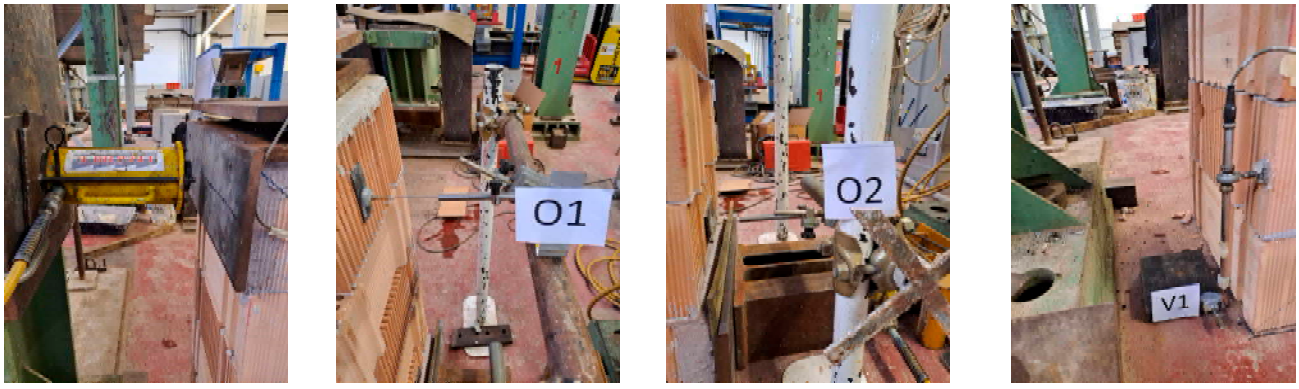

(**a**) (**b**) (**c**) (**d**)

Figure 4. Setup details of shear-compression tests: (**a**) horizontal hydraulic jack and L-shaped steel profile; (**b**) LVDT O1 attached to the top end of the wall; (**c**) LVDT O2 attached to the constrained bottom end of the wall; (**d**) LVDT V1 attached to the free bottom end.

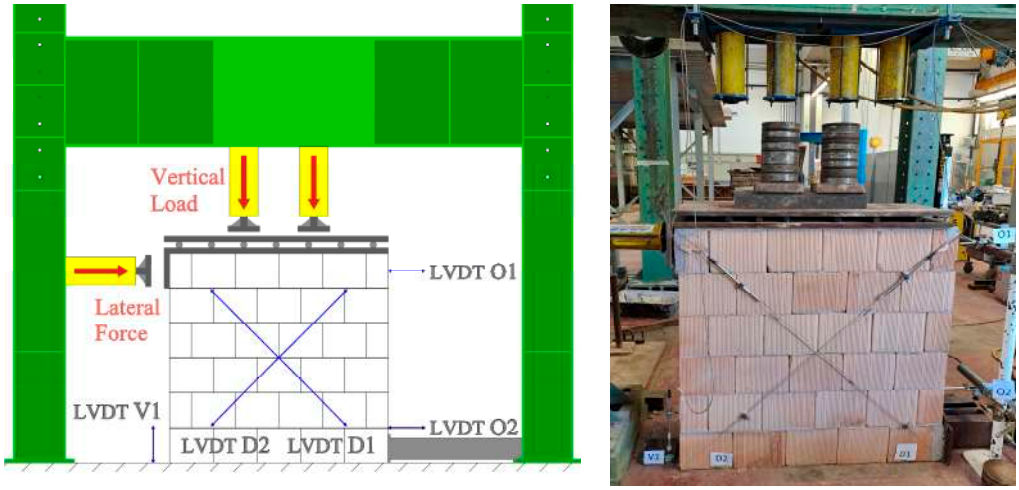

(**a**) (**b**)

Figure 5. Setup schematization (**a**) and laboratory setup (**b**) of the shear-compression tests.

4.1.2. Bending and Compression Tests on the Special Mortar

Tests were conducted on three specimens measuring 40 mm × 40 mm × 160 mm in accordance with EN 1015-11:2019 [42] to find their flexural and the compression strengths. Three-point bending tests were first performed on the three specimens, followed by compression tests on the remaining halves of the specimens after the bending tests. Figure 6 shows the setup of the experimental tests performed on the Porotherm special mortar.

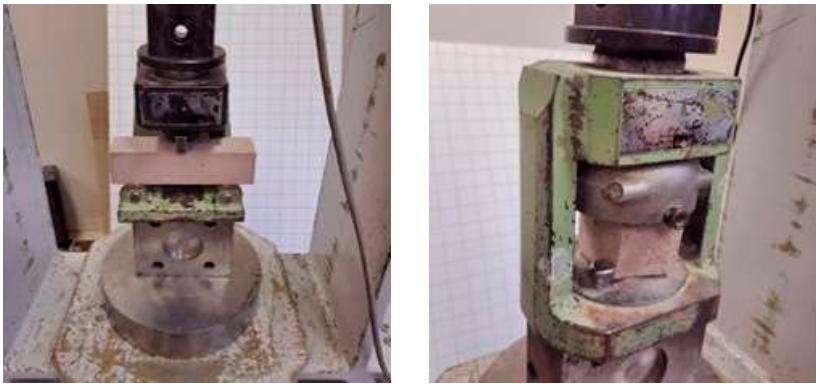

(**a**) (**b**)

Figure 6. Setup of bending tests (**a**) and compression tests (**b**) on mortar.

4.1.3. Shear Tests on Triplets

Three tests on triplets were carried out, in accordance with the provisions of EN 1052-3:2002/A1:2007 [43], in order to assess the mechanical behavior, in terms of their strength and deformation, of the horizontal joints of the "Porotherm" masonry system. The specimens (T01, T02, T03) were made with Porotherm BIO PLAN 45-25/19.9 load-bearing bricks, cut to obtain a length of 350 mm and joined with Porotherm special mortar. The tests were carried out in the absence of precompression, and the vertical force was applied by means of a hydraulic jack with a maximum load of 500 kN. A vertical displacement transducer (LVDT) was applied at the middle of the central block to record its slip. The experimental setup of the shear tests on the triplets is shown in Figure 7.

Figure 7. Setup of shear tests on triplets.

4.2. Numerical Analyses

The shear-compression tests were reproduced through FE simulations using the software ANSYS Mechanical APDL 2022 R2 [62]. The blocks were modeled using 65 solid elements, with 8 nodes each. The contact between the blocks was modeled with CONTA174 elements. The nodes at the base were fixed to the ground, while the upper nodes were constrained to avoid horizontal out-of-plane displacement of the walls. A calibration process was performed on the numerical models, aiming to represent the structural behavior exhibited by the experimental specimens. The calibration involved the following parameters: type of constitutive law; elastic modulus (E); type of contact (contact pair); imposed displacement; lateral force; Normal Penalty Stiffness; contact friction coefficient; and cohesion. All the FE models created had an initial linear–elastic range. As for the post-elastic behavior, we chose to investigate a combination of different types of constitutive laws (i.e., elastic–perfectly plastic, multilinear), damage and failure criteria (i.e., Drucker–Prager, William–Warnke [63]). An example of a FE model is shown in Figure 8. The displacement control analyses were carried out by increasing the lateral load until a maximum horizontal displacement of 50 mm.

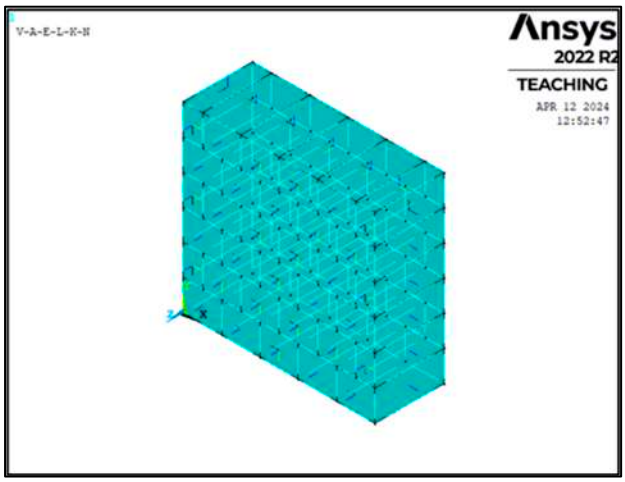

Figure 8. FE model in Ansys APDL.

4.2.1. Numerical Model 1 (M1)

In the present model, a multilinear stress (σ)–strain (ε) relationship (Figure 9) was assigned to the blocks, considering a maximum strength equal to 13.2 N/mm^2 (average compressive strength of the block, provided by the manufacturer). The failure is governed

by the William–Warnke criterion [63]. The contact between the blocks is of the "Standard" type, which prevent the blocks from slipping and separating until failure, after which they obey a frictional law (Coulomb). The friction coefficient is 0.4, while the cohesion is 0.52 N/mm^2 (shear strength in the absence of compression, provided by the manufacturer). The input parameters are listed in Table 4.

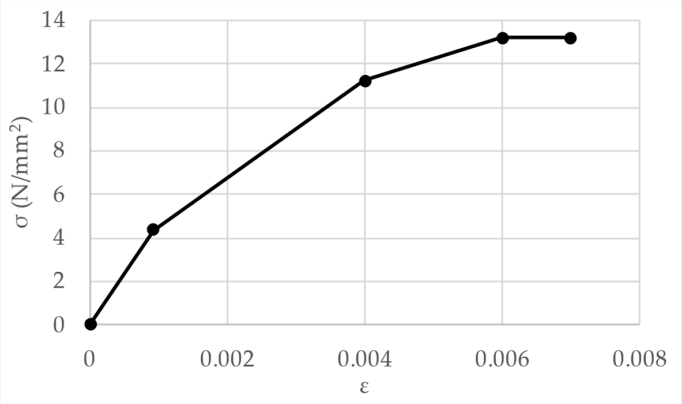

Figure 9. Stress (σ)–strain (ε) relationship of numerical model 1.

Table 4. Structural parameters of numerical model 1.

Bricks' mean compression strength	(N/mm^2)	13.2
Young's modulus	(N/mm^2)	4840
Poisson's ratio	-	0.25
Open shear transfer coefficient	-	0.2
Closed shear transfer coefficient	-	0.8
Ultimate uniaxial cracking stress	(N/mm^2)	1.32
Ultimate uniaxial crushing stress	(N/mm^2)	13.2

4.2.2. Numerical Model 2 (M2)

In the present model, an elastic–perfectly plastic multilinear stress (σ)–strain (ε) relationship was assigned to the blocks (Figure 10) up to a maximum strength of 13.2 N/mm^2 (mean compressive strength of the block provided by the manufacturer). The failure is governed by the William–Warnke criterion [63]. The contact between the blocks is of the "Rough" type, which allows the blocks to detach until failure and simulates sliding according to a frictional law (Coulomb). The friction coefficient is 0.4, while the cohesion is 0.52 N/mm^2 (shear strength in the absence of compression, provided by the manufacturer). The parameters entered are reported in Table 5.

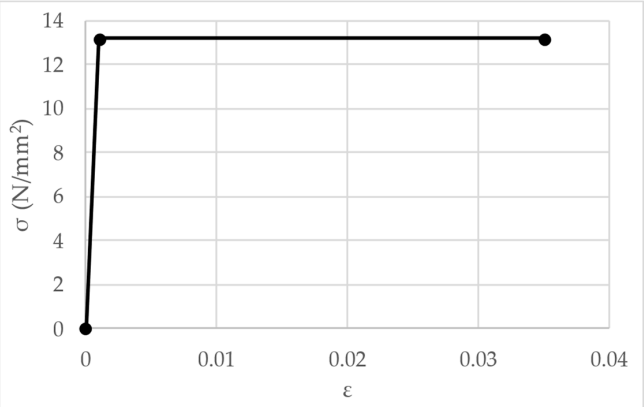

Figure 10. Stress (σ)–strain (ε) relationship of numerical model 2.

Table 5. Structural parameters of numerical model 2.

Bricks' mean compression strength	(N/mm^2)	13.2
Young's modulus	(N/mm^2)	13,200
Poisson's ratio	-	0.25
Open shear transfer coefficient	-	0.2
Closed shear transfer coefficient	-	0.8
Ultimate uniaxial cracking stress	(N/mm^2)	1.32
Ultimate uniaxial crushing stress	(N/mm^2)	13.2

4.3. Analytical Formulae from Eurocodes

The shear-compression test conditions on the masonry walls were analytically verified by means of formulae that allowed us to calculate the shear strength and maximum drift of the walls (defined as the ratio between the horizontal displacement at the top and the panel height). The analytical calculation process was aimed to check the reliability of applying the verification methods proposed in the European standards, such as EN 1996-1:2022 (Eurocode 6) [47] and EN 1998-3:2005 (Eurocode 8) [48], to the special insulating masonry system with thin joints (Porotherm). In particular, the following analytical formulae for the in-plane shear of masonry structures was considered:

$$V_t = l_c t\, f_{vd} \tag{1}$$

where V_t is the shear strength of the masonry wall according to Eurocode 6 [47]; l_c is the length of the compressed part of the wall; t is the thickness of the wall; and f_{vd} is the design shear strength of the masonry. Moreover, δ_u represents the maximum drift of the wall according to Eurocode 8 [48]:

$$\delta_u = \frac{4}{3}\, 0.004. \tag{2}$$

5. Results

The results of the study are presented separately for each type of investigation:

- Experimental;
- Numerical;
- Analytical.

5.1. Experimental Results

The results are sorted according to the performed tests. For each test, the results necessary for the structural characterization of the masonry are reported.

5.1.1. Shear-Compression Tests Results

From the shear-compression tests carried out on the three Porotherm masonry walls, it was possible to derive lateral force (F)–horizontal displacement (O1) curves, shear stress (τ)−shear strain (γ) curves and the elastic moduli of the specimens. The shear stresses τ were calculated from the applied horizontal force (F) and the area of the top face of the wall (A): $\tau = F/A$. The shear strains γ and the ultimate drift δ_u were obtained by dividing the value of the horizontal displacement at the top (O1) by the height of the walls (H): $\gamma = O1/H, \delta_u = \gamma_{max} = O1_{max}/H$. Figures 11 and 12 show the experimental curves obtained from the shear-compression tests. The markers in Figure 11 highlight the damage levels experienced by the specimens during the tests: initial damage (a); the damage level at the lateral peak load (b) and failure (c).

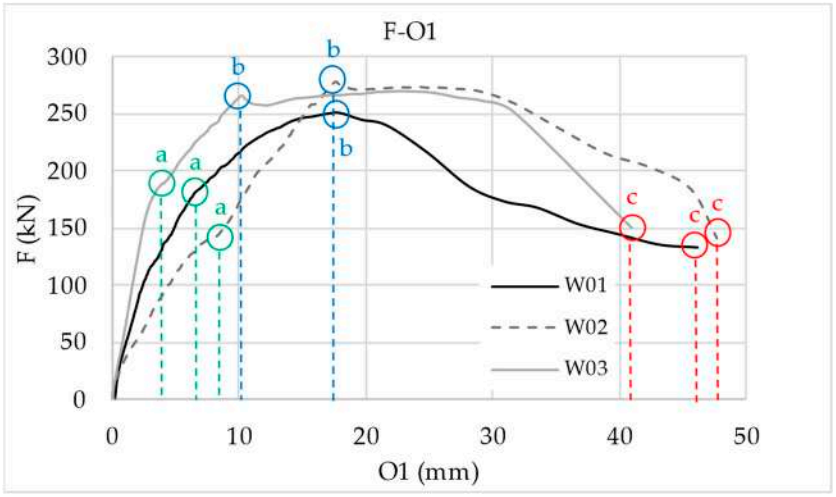

Figure 11. Force (F)–horizontal displacement (O1) curves for the three masonry specimens with the markers of the damage levels: (a) initial damage; (b) damage at the peak lateral load; (c) failure.

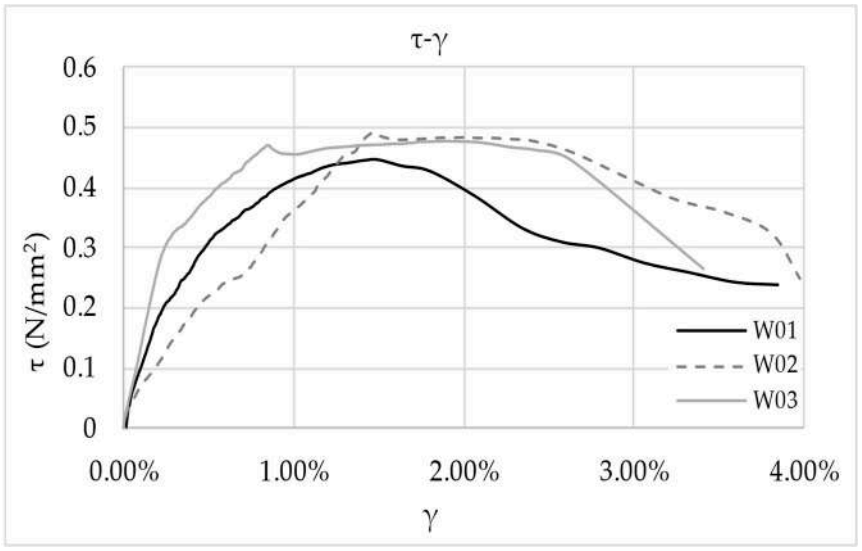

Figure 12. τ-γ curves of the three masonry specimens.

The three walls showed an initial linear branch with three different slopes, indicating a variation in stiffness among the specimens. In particular, wall W03 showed a significantly higher stiffness in the linear segment (see Table 6), and the initial damage occurred for a displacement of 3.43 mm. W01 and W02 underwent initial damage at displacement values equal to 6.57 mm and 7.51 mm, respectively. After the initial damage, the walls underwent a stiffening branch until the lateral maximum load was reached. The higher stiffness of specimen W03 was confirmed by it reaching the maximum lateral load at a displacement of 22.88 mm. The stiffness branch for W01 and W02 ended at displacement values of 17.61 mm and 17.67, respectively. A softening branch can be observed in the three walls until collapse. W02 exhibited more deformability compared to the other specimens by reaching complete failure at a displacement of 48.14 mm (O_{max} in Table 6). The tangent shear moduli (G_{tan}) were computed from the τ-γ curves by approximating the initial segment in the elastic field with a straight line. This line is defined by the trend line of the curve. The secant elastic moduli (G_{sec}) are defined by the ratio between the value of τ at the elastic limit and the corresponding value of γ. The experimental results obtained from the compression-shear tests are shown in Table 6.

Table 6. Experimental results for W01, W02 and W03.

		W01	W02	W03	Mean Value
F_{max}	kN	251.54	277.83	269.74	266.37
O_{max}	mm	46.10	48.14	40.87	47.96
τ_{max}	N/mm^2	0.32	0.25	0.32	0.30
γ (τ_{max})	%	1.47	1.47	1.91	1,62
$\tau_{elastic\ limit}$	N/mm^2	0.32	0,25	0.32	0.30
$\gamma_{elastic\ limit}$	%	0.55	0.63	0.29	0.49
δ_u	%	4.00	3.97	3.41	3.95
G_{sec}	N/mm^2	59.22	39.62	113.18	70.68
G_{tan}	N/mm^2	73.14	46.57	129.47	83.06

Figure 13 depicts the collapsed states of the three specimens, underlining their shear-dominated failure. All the walls showed coupling between the diagonal and horizontal sliding shear failures.

(**a**) (**b**) (**c**)

Figure 13. Collapsed state of W01 (**a**), W02 (**b**) and W03 (**c**).

Diagonal shear failure is related to the tensile rupture of the masonry along the compressed diagonal, while horizontal sliding shear failure, with stepped diagonal cracks, is associated with the mortar joints' failure. During the tests, cracking noises could be heard coming from the specimens immediately after the onset of the initial damage (markers "a" in Figure 11), suggesting progressive failure of the blocks' webs and shells. The horizontal slip of the bricks along the compressed diagonal is noticeable in the three walls, followed by several fractures. As shown in Figure 13a, the W01 blocks did not collapse despite the wider spread of the fractures and exhibited less significant horizontal sliding behavior. In particular, the cracking noises intensified starting from a displacement value of 17.61 mm, corresponding to the maximum lateral load (see Figure 11), and the cracks started to visibly spread on the surfaces of the wall. W02 and W03 experienced complete failure of the bricks along the compressed diagonal (Figure 13b,c), associated with remarkable horizontal sliding of several of the block units. In particular, horizontal sliding of specimens W02 and W03 started to become evident after the maximum lateral load was reached (markers "b" in Figure 11), followed by the collapse of the bricks.

5.1.2. Bending and Compression Tests on the Special Mortar

The tests carried out on the special Porotherm mortar allowed us to determine the flexural strength and compressive strength of the mortar. The flexural strength was calculated according to the formula suggested in the standard:

$$f = 1.5 \frac{F\,l}{b\,d^2} \quad (3)$$

where f is the flexural strength; F is the maximum load applied to the specimen (N); l is the span between the support rollers (mm); b is the width of the specimen (mm); and d is the depth of the specimen (mm).

Compressive strength was determined by calculating the average of the individual specimens (the two remaining segments from the flexural tests). The values of the mortar strength obtained from the tests are reported in Table 7.

Table 7. Experimental results of the tests on mortar specimens.

Flexural strength	(N/mm^2)	0.80
Compressive strength	(N/mm^2)	13.8

The compressive strength in Table 7 is perfectly consistent with that indicated in the technical data sheet provided by the producer.

5.1.3. Shear Tests on Triplets

The shear tests on the triplet specimens (T01, T02, T03) allowed us to calculate the shear strength, in the absence of compression, of the Porotherm load-bearing masonry system's horizontal joints. It was possible to derive the force–deformation curves. The average shear strength, equal to 0.39 N/mm^2, was obtained from the average of the individual sample's strengths, calculated using the following formula:

$$f_{v0i} = \frac{F_{i,max}}{2A_i} \quad (4)$$

where f_{v0i} is the shear resistance of a single sample (N/mm^2); $F_{i,max}$ is the maximum shear force (N); and A_i is the cross-sectional area of a specimen parallel to the horizontal joints (mm^2). The characteristic initial shear strength, equal to 0.31 N/mm^2, was calculated by multiplying the mean value by 0.8. Figure 14 shows the curves obtained from the tests on the triplets.

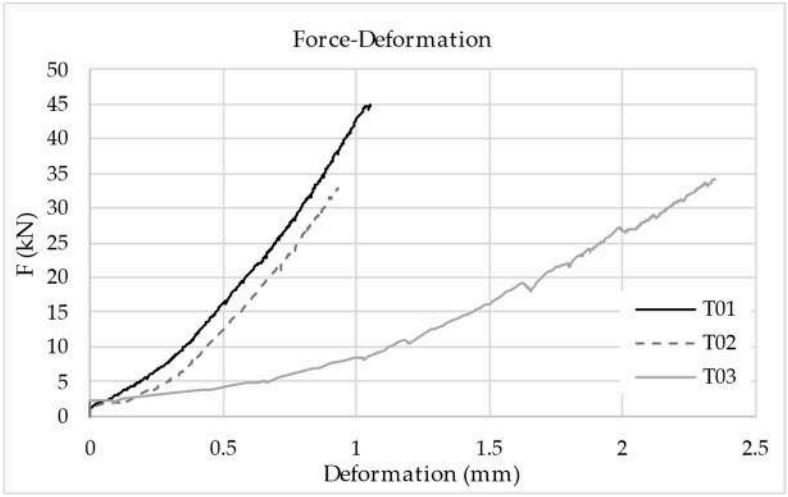

Figure 14. Force–deformation curves of shear tests on T01, T02 and T03.

Samples T01 and T02 showed similar behavior until collapse, with T01 able to reach a higher strength. Sample T03 exhibited lower stiffness, as can be seen in the slope of the curve in Figure 14, which was significantly lower than that of the others. The triplets were found to reach a collapsed state (Figure 15a) due to the failure of the mortar thin joints. All the specimens showed the same failure mechanism, with net fracture of the mortar (see Figure 15b).

(**a**) (**b**)

Figure 15. Failure mode of triplets (**a**) and mortar joint fracture (**b**).

5.2. Numerical Results

The FE simulations aimed both to reproduce the tests conducted on the Porotherm masonry walls and to build a solid model able to predict the structural behavior of such construction systems. Two numerical models were analyzed (M1 and M2) considering two different constitutive relations for the masonry and two types of contact laws at the brick interface (see Section 4.2). Lateral force (F)–horizontal displacement (O) curves, shear stress (τ)–shear strain (γ) curves and the elastic moduli of the samples were obtained. Figures 16 and 17 show the curves obtained from the FE simulations. The markers in Figure 16 highlight the damage levels experienced by the specimens during the tests: initial damage (a) and failure (b). The numerical models reached the maximum lateral load at failure.

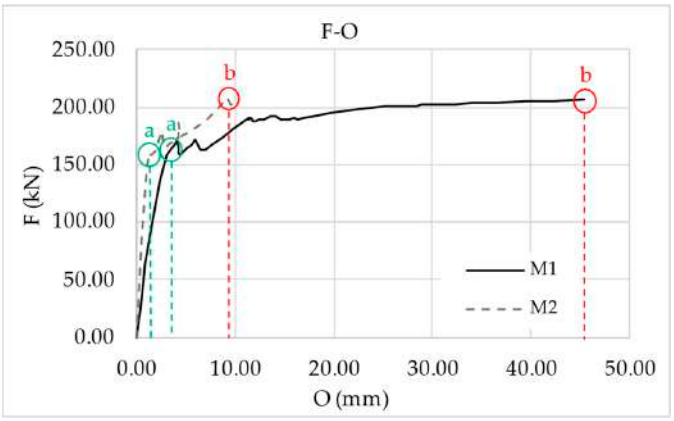

Figure 16. Force (F)–displacement (O) curves obtained from the numerical models with markers of the damage levels: (a) initial damage; (b) failure at the peak lateral load.

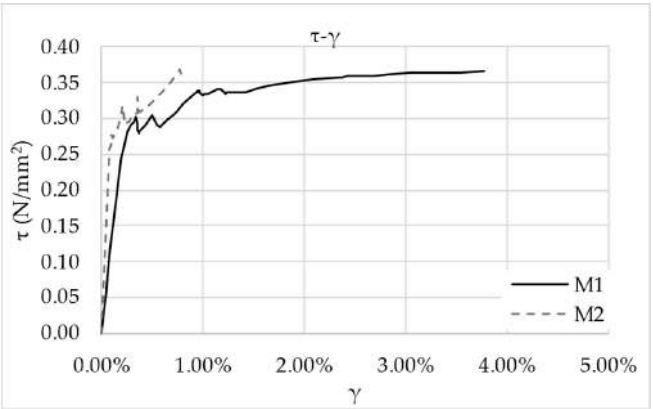

Figure 17. Shear stress (τ)–shear strain (γ) curves obtained from the numerical models.

Both models showed a very similar initial elastic response, with almost identical stiffness and linear behavior at the beginning of deformation ($\tau_{elastic\ limit}$ in Table 8). Model M2 showed a slightly higher elastic stiffness until the appearance of the initial damage, at a displacement of 1.1 mm, but a shorter plastic region, suggesting lower deformability and fragile behavior. Indeed, the maximum horizontal displacement experienced by M2 was equal to 9.75 mm (O_{max} in Table 8). Conversely, model M1 exhibited a slightly lower elastic stiffness, experiencing initial damage at a displacement equal to 3.51 mm. As shown in Figure 16, the plastic region of M1 was significantly more extensive compared to M2 and led to complete rupture at a displacement of 45.37 mm. The two models reached the same maximum shear strength value of 0.37 N/mm^2 (τ_{max} in Table 8).

Table 8. Numerical results for M1 and M2.

		M1	M2
F_{max}	kN	207.69	207.84
O_{max}	mm	45.37	9.75
τ_{max}	N/mm^2	0.37	0.37
γ (τ_{max})	%	4.00	0.77
$\tau_{elastic\ limit}$	N/mm^2	0.29	0.27
$\gamma_{elastic\ limit}$	%	0.29	0.09
δ_u	%	4.84	0.81
G_{sec}	N/mm^2	99.37	291.75
G_{tan}	N/mm^2	110.97	310.91

Table 8 shows the numerical results obtained from the FE simulations performed on models M1 and M2.

The Von Mises stress plots in Figure 18 highlight the consistency of the stress distributions with the failure modes observed in the shear-compression tests (see Section 5.1.1). Both M1 (Figure 18a) and M2 (Figure 18b) show the horizontal sliding and shear deformation of several bricks. The stresses are increased along the compressed diagonal and are spread across the adjoining bricks. Furthermore, the intensification of the stresses led to failure and hence to the detachment of the joints.

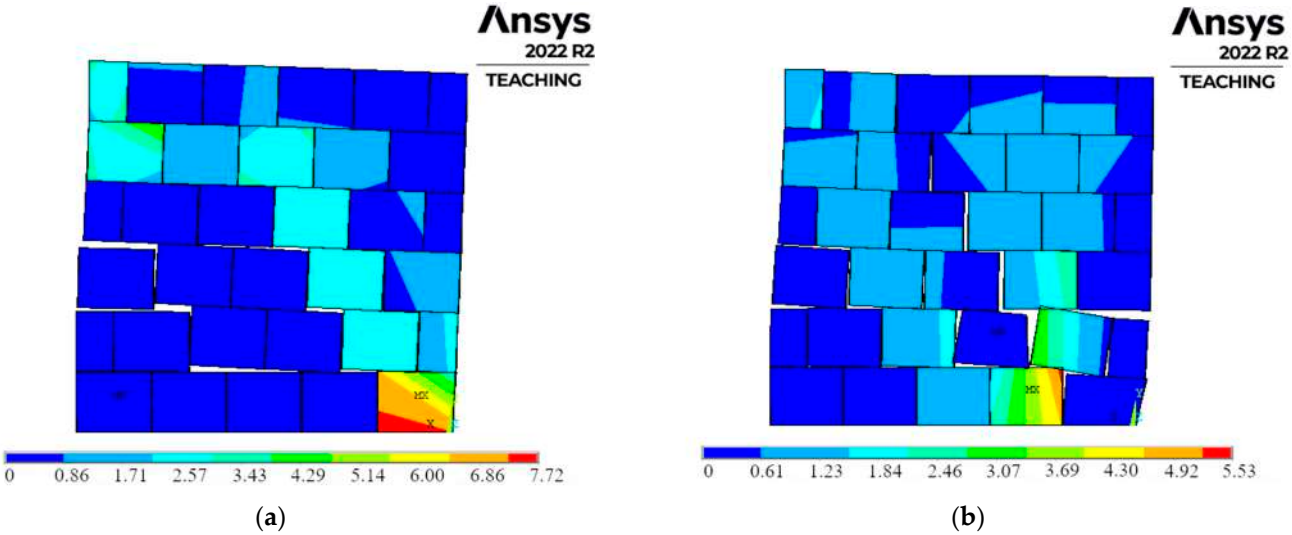

Figure 18. Von Mises stress maps (N/mm^2) of model M1 (**a**) and model M2 (**b**).

5.3. Analytical Results

The present section presents an analytical evaluation of the most relevant structural parameters of the masonry walls. The compressed length of the wall (l_c) in Equation (1) was obtained by means of the eccentricity (e) of the vertical load (N) at the base, resulting from

the moment generated by the horizontal force (V) at a height (H) of 1190 mm: $e = VH/N$. The horizontal force (V) was taken as equal to 168.09 kN, which corresponds to the mean experimental values at which damage occurs. The vertical force was chosen in order to obtain a compression stress of 0.62 N/mm^2, reproducing the experimental conditions. l_c was then obtained considering the linear stress distribution of the compressive stresses from the following relation, with l being the total length of the wall:

$$l_c = \begin{cases} l, & e \leq l/6 \\ 3\left(\frac{1}{2} - e\right), & e > l/6 \end{cases} \quad (5)$$

The ultimate drift (δ_u) is crucial for understanding the deformation and ductility of the wall. Table 9 presents the shear resistance (V_t) and the ultimate drift (δ_u).

Table 9. Analytical evaluation of structural parameters.

	Standard		
V_t	Eurocode 6 [47]	90.91	kN
δ_u	Eurocode 8 [48]	0.5	%

6. Discussion

With this being a preliminary experimental investigation on a sustainable innovative load-bearing masonry system, the choice of the specimens' size and scale was made for practical and time- and cost-saving reasons. Scaling of masonry's structural components and structure is rather challenging, and often, differences in the stiffness, strength and failure mechanisms between different-sized masonries can be found (see, e.g., [44–46] and the references therein). As pointed out in [46], comparing the results from full-scale wall panels to those from half-scale wall panels with full-scale bricks, a slight reduction in the measured shear stiffness and a modest increase in their shear strength were highlighted. More precisely, in Lu and Kasa [53], two wallettes, with dimensions of 2500 mm (width) × 1750 mm (height) × 300 mm (thickness) and constructed with Porotherm 30-S, were tested in terms of their shear-compression until failure. These masonry walls can be considered the full-size versions of our specimens. The results showed that the registered maximum shear load (250 kN) is about 6% lower than the mean value (266.37 kN) in the present research, and the ultimate drifts are quite similar, varying from 5% to 6%. As an extension of our work, it is reasonable to deduce that the scale effect could have affected both the strength and stiffness values, with moderate but still acceptable deviations.

The experimental results reveal critical insights into the mechanical behavior of Porotherm masonry walls. The shear-compression tests showed slightly different stiffnesses and strengths among the specimens, while the failure mechanism observed was the same, namely a combination of diagonal shear and sliding shear failures. Wall W03 exhibited the highest initial stiffness, as evidenced by the steep slope of the force–displacement curve, while wall W01 displayed the longest softening branch, indicating a higher displacement capacity (see Figure 11). These variations suggest that the manufacturing process may influence the performance of thin joint masonry walls.

The bending and compression tests on the special Porotherm mortar exhibited a flexural strength of 0.80 N/mm^2 and a compressive strength of 13.8 N/mm^2. These experimental values are consistent with those provided in the producer's technical data sheets.

Shear tests on the triplet specimens provided additional data on the shear strength of the masonry's horizontal joints. The average shear strength was calculated to be 0.39 N/mm^2, with a characteristic initial shear strength of 0.31 N/mm^2 after applying a reduction factor. The force–deformation curves indicated that samples T01 and T02 behaved similarly until failure, whereas T03 exhibited a significantly lower stiffness. The triplets reached a collapsed state due to the failure of the thin mortar joints.

The experimental shear-compression tests were simulated using two FE numerical models (M1 and M2) with different constitutive laws (multilinear hardening for M1 and elastic–perfectly plastic for M2) and different brick-to-brick contact types ("Standard" for M1 and "Rough" for M2). Both models showed the same shear strength, at 0.37 N/mm^2, while M1 showed a higher elastic stiffness, with G_{sec} and G_{tan}, respectively, being 193.6% and 180.17% higher than the corresponding values of model M1.

Figure 19 depicts a comparison between the experimental, numerical and analytical results in terms of the masonry's shear capacity and ultimate drift.

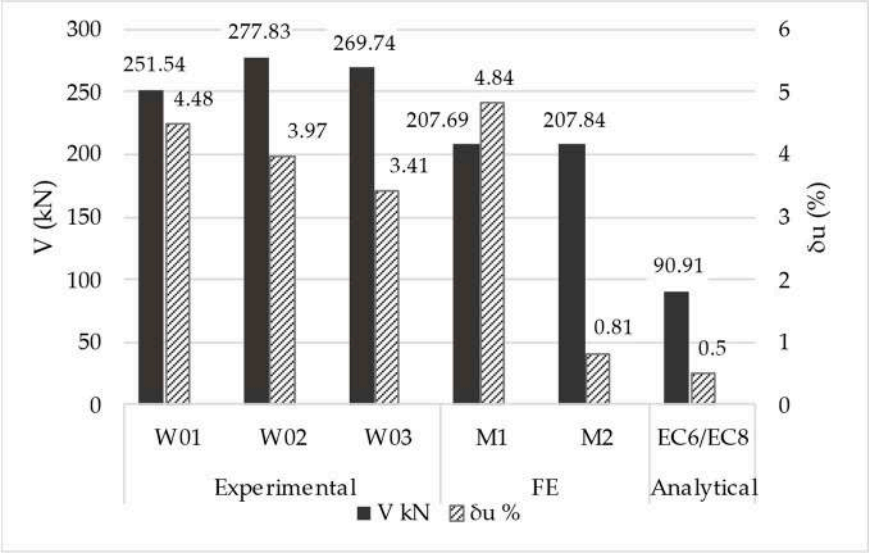

Figure 19. Comparison in terms of shear strength (V) and ultimate drift (δ_u).

By comparing the results in terms of shear strength, it can be noticed that both M1 and M2 approximate the corresponding experimental mean value (266.37 kN) well, with a deviation of about 28%. On the contrary, looking at the displacement capacity δ_u, the ultimate drift of the M2 model is about 388% lower than the experimental mean value (3.95%) and is of the same order of magnitude as the Eurocode value. Meanwhile, M1's numerical value is a better approximation with respect to the experimental results, with a deviation of 22.5%. As illustrated in Figure 18, both numerical models properly reproduce the experimental damage mechanisms. The computational findings suggest that the combination of a multilinear stress–strain constitutive relation for the blocks, coupled with the William–Warnke yield criterion and a standard contact frictional law, leads to a better numerical approximation of the experimental in-plane shear behavior of the masonry walls in terms of their shear strength and ultimate drift. Moreover, in order to improve the numerical results, a final softening branch could be added to the multilinear curve.

The analytical evaluations, based on the Eurocode standards [47,48], provided benchmark values for the design and analysis of the masonry walls. The results obtained from both the experimental and numerical analyses significantly exceed the shear strength values evaluated through the analytical methods proposed by Eurocodes 6 and 8. In particular, the shear strengths (V) in the experimental tests and numerical simulations were, at a minimum, 53% and 26.4% higher, respectively, than those calculated by means of the analytical methods. As also pointed out in other previous works [21,30], Equation (1), used in the case of sliding shear failure, significantly underestimates the experimental results and could provide a lower bound for the shear strength. Similar non-compliance was also noticed between the ultimate drift capacity values, a key indicator of the ductility of masonry. Both the experimental and numerical analyses indicated ultimate drifts that were notably higher compared to the values obtained by following the Eurocode standards. Thus, the analytical values for shear resistance and ultimate displacements developed in the Eurocodes on the

basis of the sliding shear mechanism do not provide accurate information regarding the shear properties of masonry walls.

Table 10 presents a comparison between the present research and other experimental papers on the in-plane shear-compression behavior of clay brick masonry walls. These research works have been selected by considering similar masonry types, dimensions and precompression loads as much as possible. In the table, λ represents the slenderness ratio, σ_0 is the vertical precompression, $V_{max,\,mean}$ is the mean value of the maximum horizontal load and $\tau_{max,\,mean}$ is the mean value of the maximum shear stress. The failure modes are classified as follows: TDS for tensile diagonal shear failure, F for flexural failure and HSS for horizontal sliding shear failure.

Table 10. Experimental campaigns on shear-compression tests performed on masonry walls [30].

Authors	Masonry Type	Dimensions l/H/t (mm)	λ (H/l)	σ_0 (N/mm^2)	Mortar Joints (Thin/Thick)	Failure Mode	$V_{max,\,mean}$ (kN)	$\tau_{max,\,mean}$ (N/mm^2)
Tomaževič (2009) [21]	Hollow clay bricks	990/1420/290	1.43	1	thick	TDS	93.9	0.33
	Hollow clay bricks	990/1420/290	1.43	1.62	thick	TDS	141.7	0.49
Salmanpour et al. (2015) [7]	Hollow clay bricks	1500/1600/150	1.07	0.64	thick	TDS	91	0.4
	Hollow clay bricks	1500/1600/150	1.07	0.96	thick	TDS	103	0.46
Martinelli et al. (2016) [64]	Solid clay bricks	1160/1160/250	1	0.52	thick	TDS	64.33	0.34
Lourenço et al. (2010) [16]	Perforated clay bricks	1200/1090/300	0.9	0.375	thick	F	71.8	0.20
Present research	Hollow clay bricks	1250/1190/450	0.95	0.62	thin	HSS/TDS	266.37	0.3

As can be noticed, the maximum shear load $V_{max,\,mean}$ for the present masonry wall is much greater than the values for other hollow/perforated brick masonries and also solid clay brick masonries. The range of the increase varies from 56% compared to that in Tomaževič [21] (hollow clay bricks) to 75% compared to that in Martinelli et al. [64] (solid clay bricks). The failure modes are strongly influenced not only by the size and scale of the walls but also by the thickness of the mortar joints and the mechanical properties of the mortar. Even though the damage mechanism is a combination of HSS and TDS, highlighting a likely weakness point within the horizontal thin mortar joints, it is possible to confirm the significant load-bearing shear capacity of this innovative masonry system. Moreover, the value for the maximum shear stress $\tau_{max,\,mean}$ is consistent with that for the other masonry types due to high thickness of the panel, and it can be used in nonlinear static FE analyses of masonry buildings.

7. Conclusions

In the present research, three load-bearing Porotherm masonry walls were tested under lateral increasing loads and a constant vertical precompression load in order to characterize their in-plane shear behavior. The specimens were made with innovative load-bearing block units with high thermal insulation. Structural characterization of the special Porotherm mortar used for the horizontal thin joints was performed. The shear strength of the horizontal thin joints was evaluated through experimental tests on three triplets. Two FE models of the shear-compression tests, using different constitutive laws and brick-to-brick contact types, were built and calibrated on the experimental results. Furthermore, the shear strength and the drift capacity were estimated through the analytical methods proposed by the current European standards. The results focused on the evaluation of the shear strength, the ultimate drift and damage mechanisms of the masonry walls and their accordance with the Eurocode standards.

Based on the results obtained from the experimental, numerical and analytical investigations, the following conclusions can be drawn:

(1) The experimental results showed a high value for the maximum shear load (266.37 kN) reached in the in-plane shear-compression tests. As reported in Table 10, it can be

noticed that the maximum shear load presents a relevant increase, ranging from 57% (hollow clay bricks) to 75% (solid clay bricks), compared to other similar masonry types with analogous dimensions and precompression loads. This suggests that the present load-bearing Porotherm masonry system with thin horizontal joints represents a valid alternative to traditional or other hollow clay brick masonry systems under seismic actions.

(2) The experimental campaign also highlighted shear-dominated behavior in the collapsed state. The diagonal shear damage was coupled with horizontal shear sliding, with stepped diagonal cracks, underlining a plausible weakness of the thin horizontal mortar joints. This result can also be confirmed by the shear tests on the triplets. The bond of the thin mortar joints can be enhanced by the use, for instance, of fiber-reinforced composites [14] or polymer–cement [15].

(3) Comparison between the experimental and numerical results (Figure 19) proved that the use of a multilinear stress–strain constitutive relation for the blocks, with a William–Warnke yield criterion and a contact frictional law, led to a better numerical approximation of the experimental in-plane shear behavior of the masonry walls in terms of their shear strength and ultimate drift. To improve the numerical results, a final softening branch could be added to the multilinear constitutive curve.

(4) Comparison between the experimental and analytical results (Figure 19) showed that the Eurocode values for shear resistance and ultimate displacement, based on the sliding shear mechanism, do not provide accurate information regarding the shear properties of masonry walls. Indeed, the shear strength in the experimental tests was found to be 53% higher than that calculated by means of the analytical methods. The European standards provide an underestimation of both shear strength and drift capacity, which can be used as lower bounds in applications. Therefore, experimental campaigns are crucial to identify the maximum shear load, drift and corresponding failure mode of masonry walls.

The experimental and numerical results proved the structural potential of the masonry systems studied as load-bearing shear walls, showing a significant shear strength and drift capacity. Furthermore, the present Porotherm masonry offers additional benefits in terms of sustainability due to the presence of recycled wooden powder in the brick compound and enhanced thermal insulation. Thus, in addition to being a suitable and potential eco-friendly building system that is beneficial for the environment, energy-efficient and cost-effective, the present Porotherm masonry also represents a valid alternative to traditional masonry systems from a structural point of view.

Finally, with this being a preliminary experimental and numerical investigation on this type of load-bearing masonry, it will be crucial to program a future experimental campaign on full-scale panels and test structures and implement more advanced and extensive FE simulations in order to obtain a better understanding of their structural seismic performance.

Author Contributions: Conceptualization, M.S. and A.C.; methodology, M.S., A.C. and F.S.; software, A.C.; validation, M.S. and A.C.; formal analysis, M.S. and A.C.; investigation, M.S. and A.C.; resources, M.S.; data curation, M.S. and A.C.; writing—original draft preparation, M.S., A.C. and F.S.; writing—review and editing, M.S., A.C. and F.S.; supervision, M.S. and F.S. All authors have read and agreed to the published version of the manuscript.

Funding: This research received no external funding.

Data Availability Statement: Data, models and codes that support the findings of this study are available from the corresponding author upon reasonable request.

Acknowledgments: The authors wish to thank Wienerberger S.p.a. for having provided the components of the masonry for the experimental campaign. The experiments were carried out at the "Laboratorio Ufficiale Prove Materiali e Strutture—Prof. Giovanni Menditto" of the Dept. of Civil and Building Engineering and Architecture, Università Politecnica delle Marche. The technical support of Andrea Conti, Franco Rinaldi and Carlo Perticarini was greatly appreciated.

Conflicts of Interest: The authors declare no conflicts of interest.

References

1. IEA. *Perspectives for Clean Energy Transition. The Critical Role of Buildings*; IEA: Paris, France, 2019.
2. Zhao, Y.; Liu, L.; Yu, M. Comparison and Analysis of Carbon Emissions of Traditional, Prefabricated, and Green Material Buildings in Materialization Stage. *J. Clean. Prod.* **2023**, *406*, 137152. [CrossRef]
3. Stazi, F.; Serpilli, M.; Chiappini, G.; Pergolini, M.; Fratalocchi, E.; Lenci, S. Experimental Study of the Mechanical Behaviour of a New Extruded Earth Block Masonry. *Constr. Build. Mater.* **2020**, *244*, 118368. [CrossRef]
4. Serpilli, M.; Stazi, F.; Chiappini, G.; Lenci, S. Earthen Claddings in Lightweight Timber Framed Buildings: An Experimental Study on the Influence of Fir Boards Sheathing and GFRP Jacketing. *Constr. Build. Mater.* **2021**, *285*, 122896. [CrossRef]
5. Briga-Sá, A.; Silva, R.A.; Gaibor, N.; Neiva, V.; Leitão, D.; Miranda, T. Mechanical Characterization of Masonry Built with ICEBs of Granite Residual Soils with Cement–Lime Stabilization. *Buildings* **2022**, *12*, 1419. [CrossRef]
6. Messali, F.; Esposito, R.; Ravenshorst, G.J.P.; Rots, J.G. Experimental Investigation of the In-Plane Cyclic Behaviour of Calcium Silicate Brick Masonry Walls. *Bull. Earthq. Eng.* **2020**, *18*, 3963–3994. [CrossRef]
7. Salmanpour, A.H.; Mojsilović, N.; Schwartz, J. Displacement Capacity of Contemporary Unreinforced Masonry Walls: An Experimental Study. *Eng. Struct.* **2015**, *89*, 1–16. [CrossRef]
8. Lachheb, M.; Youssef, N.; Younsi, Z. A Comprehensive Review of the Improvement of the Thermal and Mechanical Properties of Unfired Clay Bricks by Incorporating Waste Materials. *Buildings* **2023**, *13*, 2314. [CrossRef]
9. Cavaco, E.; Grilo, I.; Paulo Gouveia, J.; Júlio, E.; Neves, L. Mechanical Performance of Eco-Efficient Hollow Clay Bricks Incorporating Industrial Nano-Crystalline Aluminium Sludge. *Eur. J. Environ. Civ. Eng.* **2020**, *24*, 1921–1938. [CrossRef]
10. Foti, D.; Lerna, M.; Vacca, V. Experimental Characterization of Traditional Mortars and Polyurethane Foams in Masonry Wall. *Adv. Mater. Sci. Eng.* **2018**, *2018*, 8640351. [CrossRef]
11. Harith, I.K.; Abdulhadi, A.M.; Majdi, A. Improvement of Clay Brick Masonry Bonding Using Polyurethane Foam Mortars with Blended Cement. *Int. J. Sustain. Build. Technol. Urban Dev.* **2023**, *14*, 46–62. [CrossRef]
12. Gams, M.; Triller, P.; Jäger, A. In-Plane Seismic Behaviour of Urm and Confined Masonry Built from Vertically Perforated Blocks and Polyurethane Glue. *Structures* **2023**, *58*, 105528. [CrossRef]
13. Mojsilović, N.; Petrović, M.; Anglada, X.R. Masonry Elements with Multi-Layer Bed Joints: Behaviour under Monotonic and Static-Cyclic Shear. *Constr. Build. Mater.* **2015**, *100*, 149–162. [CrossRef]
14. Ranjan, N.; Banerjee, S.; Nayak, S.; Das, S. Exploring Applicability of Recycled Nylon Fiber Reinforced Mortar in Joints and Plaster to Enhance the Bond Strength, in-Plane and out-of-Plane Capacity of Masonry Structures. *J. Build. Eng.* **2023**, *72*, 106744. [CrossRef]
15. Thamboo, J.A.; Dhanasekar, M. Characterisation of Thin Layer Polymer Cement Mortared Concrete Masonry Bond. *Constr. Build. Mater.* **2015**, *82*, 71–80. [CrossRef]
16. Lourenço, P.B.; Vasconcelos, G.; Medeiros, P.; Gouveia, J. Vertically Perforated Clay Brick Masonry for Loadbearing and Non-Loadbearing Masonry Walls. *Constr. Build. Mater.* **2010**, *24*, 2317–2330. [CrossRef]
17. da Porto, F.; Mosele, F.; Modena, C. Compressive Behaviour of a New Reinforced Masonry System. *Mater. Struct.* **2011**, *44*, 565–581. [CrossRef]
18. Liu, X.; Li, Y.; Liu, A.; Yue, X.; Li, T. Effect of North Wall Materials on the Thermal Environment in Chinese Solar Greenhouse (Part A: Experimental Researches). *Open Phys.* **2019**, *17*, 752–767. [CrossRef]
19. Colmenares, A.P.; Sánchez, J.; Díaz, C.X. Comparative Thermal Analysis of Extruded Ceramic Products between Multi Perforated Brick and Modified Bricks in Cells Distribution. *J. Phys. Conf. Ser.* **2019**, *1386*, 012130. [CrossRef]
20. Ali, A.; Zhang, C.; Bibi, T.; Sun, L. Experimental Investigation of Sliding-Based Isolation System with Re-Centering Functions for Seismic Protection of Masonry Structures. *Structures* **2024**, *60*, 105871. [CrossRef]
21. Tomaževič, M. Shear Resistance of Masonry Walls and Eurocode 6: Shear versus Tensile Strength of Masonry. *Mater. Struct.* **2009**, *42*, 889–907. [CrossRef]
22. Tomaževič, M.; Lutman, M.; Bosiljkov, V. Robustness of Hollow Clay Masonry Units and Seismic Behaviour of Masonry Walls. *Constr. Build. Mater.* **2006**, *20*, 1028–1039. [CrossRef]
23. Tomaževič, M.; Weiss, P. Robustness as a Criterion for Use of Hollow Clay Masonry Units in Seismic Zones: An Attempt to Propose the Measure. *Mater. Struct.* **2012**, *45*, 541–559. [CrossRef]
24. Calderón, S.; Sandoval, C.; Araya-Letelier, G.; Aguilar, V. A Detailed Experimental Mechanical Characterization of Multi-Perforated Clay Brick Masonry. *J. Build. Eng.* **2023**, *63*, 105505. [CrossRef]
25. Labò, S.; Marini, A. In-Plane Flexural Behavior of Hollow Brick Masonry Walls with Horizontal Holes. *Eng. Struct.* **2022**, *273*, 115086. [CrossRef]
26. Sandoval, C.; Calderón, S.; Almazán, J.L. Experimental Cyclic Response Assessment of Partially Grouted Reinforced Clay Brick Masonry Walls. *Bull. Earthq. Eng.* **2018**, *16*, 3127–3152. [CrossRef]
27. Calderón, S.; Sandoval, C.; Araya-Letelier, G.; Inzunza, E.; Arnau, O. Influence of Different Design Parameters on the Seismic Performance of Partially Grouted Masonry Shear Walls. *Eng. Struct.* **2021**, *239*, 112058. [CrossRef]
28. Perez Gavilan, J.J.; Flores, L.E.; Alcocer, S.M. An Experimental Study of Confined Masonry Walls with Varying Aspect Ratios. *Earthquake Spectra* **2015**, *31*, 945–968. [CrossRef]

29. Qin, C.; Bai, G.; Wu, T.; Wang, B.; Fu, G. Seismic Behavior of Unreinforced and Confined Masonry Walls Using Innovative Sintered Insulation Shale Blocks under Cyclic In-Plane Loading. *Constr. Build. Mater.* **2021**, *268*, 121063. [CrossRef]
30. Celano, T.; Argiento, L.U.; Ceroni, F.; Casapulla, C. Literature Review of the In-Plane Behavior of Masonry Walls: Theoretical vs. Experimental Results. *Materials* **2021**, *14*, 3063. [CrossRef]
31. Valente, M.; Milani, G. Damage Assessment and Partial Failure Mechanisms Activation of Historical Masonry Churches under Seismic Actions: Three Case Studies in Mantua. *Eng. Fail. Anal.* **2018**, *92*, 495–519. [CrossRef]
32. Clementi, F. Failure Analysis of Apennine Masonry Churches Severely Damaged during the 2016 Central Italy Seismic Sequence. *Buildings* **2021**, *11*, 58. [CrossRef]
33. Clementi, F.; Gazzani, V.; Poiani, M.; Lenci, S. Assessment of Seismic Behaviour of Heritage Masonry Buildings Using Numerical Modelling. *J. Build. Eng.* **2016**, *8*, 29–47. [CrossRef]
34. Betti, M.; Galano, L.; Vignoli, A. Time-History Seismic Analysis of Masonry Buildings: A Comparison between Two Non-Linear Modelling Approaches. *Buildings* **2015**, *5*, 597–621. [CrossRef]
35. Ip, K.; Dizhur, D.; Sorrentino, L.; Masia, M.; Griffith, M.; Ingham, J. Critical Review of Numerical Modelling Techniques for Seismic Response of Complex URM Buildings. In Proceedings of the 10th Australasian Masonry Conference, Sidney, NSW, Australia, 11–14 February 2018.
36. Garcia-Ramonda, L.; Pelà, L.; Roca, P.; Camata, G. Experimental and Numerical Insights on the In-Plane Behaviour of Unreinforced and TRM/SRG Retrofitted Brick Masonry Walls by Diagonal Compression and Shear-Compression Testing. *Constr. Build. Mater.* **2023**, *402*, 132997. [CrossRef]
37. Aref, A.J.; Dolatshahi, K.M. A Three-Dimensional Cyclic Meso-Scale Numerical Procedure for Simulation of Unreinforced Masonry Structures. *Comput. Struct.* **2013**, *120*, 9–23. [CrossRef]
38. Tariq, H.; Najafgholipour, M.A.; Sarhosis, V.; Milani, G. In-Plane Strength of Masonry Wall Panels: A Comparison between Design Codes and High-Fidelity Models. *Structures* **2023**, *47*, 1869–1899. [CrossRef]
39. Sandoval, C.; Arnau, O. Experimental Characterization and Detailed Micro-Modeling of Multi-Perforated Clay Brick Masonry Structural Response. *Mater. Struct.* **2017**, *50*, 34. [CrossRef]
40. Kamrava, A.R.; Najafgholipour, M.A.; Fathi, F. A Numerical Investigation on the In-Plane Behavior of Perforated Unreinforced Masonry Walls. *Iran. J. Sci. Technol. Trans. Civ. Eng.* **2021**, *45*, 545–560. [CrossRef]
41. D'Altri, A.M.; de Miranda, S.; Castellazzi, G.; Sarhosis, V. A 3D Detailed Micro-Model for the in-Plane and out-of-Plane Numerical Analysis of Masonry Panels. *Comput. Struct.* **2018**, *206*, 18–30. [CrossRef]
42. *EN 1015-11:2019*; Methods of Test for Mortar for Masonry—Part 11: Determination of Flexural and Compressive Strength of Hardened Mortar. European Committee for Standardization (CEN): Brussels, Belgium, 2019.
43. *EN 1052-3:2002/A1:2007*; Methods of Test for Masonry—De-Termination of Initial Shear Strength. European Committee for Standardization (CEN): Brussels, Belgium, 2003.
44. Tomaževič, M. Dynamic Modelling of Masonry Buildings: Storey Mechanism Model as a Simple Alternative. *Earthq. Eng. Struct. Dyn.* **1987**, *15*, 731–749. [CrossRef]
45. Petry, S.; Beyer, K. Scaling Unreinforced Masonry for Reduced-Scale Seismic Testing. *Bull. Earthq. Eng.* **2014**, *12*, 2557–2581. [CrossRef]
46. Knox, C.L.; Dizhur, D.; Ingham, J.M. Experimental Study on Scale Effects in Clay Brick Masonry Prisms and Wall Panels Investigating Compression and Shear Related Properties. *Constr. Build. Mater.* **2018**, *163*, 706–713. [CrossRef]
47. *EN 1996-1-1: 2022*; Eurocode 6—Design of Masonry Structures—Part-1-1: General Rules for Reinforced and Unreinforced Masonry Structures. European Committee for Standardization (CEN): Brussels, Belgium, 2022.
48. *EN 1998-3: 2005*; Eurocode 8. Design of Structures for Earthquake Resistance—Part 3: Assessment and Retrofitting of Buildings. European Committee for Standardization (CEN): Brussels, Belgium, 2005.
49. Arif Kamal, M.; Suresh Chomal, N. Assessing the Potential of Porotherm Clay Bricks as a Walling Material in Building Construction. *Am. J. Civ. Eng. Archit.* **2024**, *12*, 86–90. [CrossRef]
50. Makrygiannis, I.; Karalis, K. Optimizing Building Thermal Insulation: The Impact of Brick Geometry and Thermal Coefficient on Energy Efficiency and Comfort. *Ceramics* **2023**, *6*, 1449–1466. [CrossRef]
51. Giuffrida, G.; Dipasquale, L.; Pulselli, R.M.; Caponetto, R. Compared Environmental Lifecycle Performances of Earth-Based Walls to Drive Building Envelope Design. *Sustainability* **2024**, *16*, 1367. [CrossRef]
52. Zhangabay, N.; Bakhbergen, S.; Aldiyarov, Z.; Tursunkululy, T.; Kolesnikov, A. Analysis of Thermal Efficiency of External Fencing Made of Innovative Ceramic Blocks. *Constr. Mater. Prod.* **2024**, *7*, 1. [CrossRef]
53. Lu, S.; Kasa, M. Seismic test program of special designed clay blocks due to earthquake resistance by wienerberger consisting real scale shaking table-, cyclic shear-, diagonal tension-and compression tests. In Proceedings of the 14th World Conference on Earthquake Engineering, Beijing, China, 12–17 October 2008.
54. Morandi, P.; Magenes, G.; Albanesi, L. Mechanical characterization of different typologies of masonry made with thin shell/web clay units. In Proceedings of the 12th Canadian Masonry Symposium, Vancouver, BC, Canada, 2–5 June 2013.
55. Mendes, L.; Candeias, P.; Correia, A.; Campos Costa, A.; Coelho, E.; Jäger, A.; Lu, S.; Degée, H.; Mordant, C. Full-scale seismic testing of modern unreinforced thermal insulation clay block masonry houses. In Proceedings of the 9th International Masonry Conference 2014 in Guimarães, Guimarães, Portugal, 7–9 July 2014.

56. Partene, E.; Fekete-Nagy, L.; Stoian, V. Evaluation Of Shear Capacity For Brick Masonry Walls. *J. Appl. Eng. Sci.* **2015**, *5*, 69–74. [CrossRef]
57. Schermer, D.; Schmalz, J.; Meyer, U.J.; Gams, M.; Lutman, M.; Triller, P. Shear Tests on Thermal Insulating Clay Unit Masonry Walls with Thin Layer Mortar. *Mauerwerk* **2018**, *22*, 385–398. [CrossRef]
58. Sathiparan, N.; Anusari, M.K.N.; Samindika, N.N. Effect of Void Area on Hollow Cement Masonry Mechanical Performance. *Arab. J. Sci. Eng.* **2014**, *39*, 7569–7576. [CrossRef]
59. *EN 771-1:2011+A1:2015*; Specification for Masonry Units—Part 1: Clay Masonry Units. European Committee for Standardization (CEN): Brussels, Belgium, 2015.
60. *EN 1745:2020*; Masonry and Masonry Products—Methods for Determining Thermal Properties. European Committee for Standardization (CEN): Brussels, Belgium, 2020.
61. *EN 998-2:2016*; Specification for Mortar for Masonry—Part 2: Masonry Mortar. European Committee for Standardization: Brussels, Belgium, 2016.
62. ANSYS Mechanical APDL f2022 R2. Available online: https://www.ansys.com/academic/terms-and-conditions#tab1-1 (accessed on 10 September 2024).
63. William, K.J.; Warnke, E.P. Constitutive Model for the Triaxial Behaviour of Concrete. 1974. Available online: https://www.e-periodica.ch/digbib/view?pid=bse-re-001:1974:19::40#545 (accessed on 1 February 2024).
64. Martinelli, E.; Perri, F.; Sguazzo, C.; Faella, C. Cyclic Shear-Compression Tests on Masonry Walls Strengthened with Alternative Configurations of CFRP Strips. *Bull. Earthq. Eng.* **2016**, *14*, 1695–1720. [CrossRef]